2024 IEEE International Conference on Robotics and Automation (ICRA 2024)
May 13-17, 2024. Yokohama, Japan

Point-Wise Vibration Pattern Production via a Sparse Actuator Array for Surface Tactile Feedback

Xiaosa Li†, Runze Zhao†, Chengyue Lu, Xiao Xiao and Wenbo Ding*

***Abstract*— Surface vibration tactile feedback is capable of conveying various semantic information to humans via handheld electronic devices, such as smartphones, touch panels, and game controllers. However, covering the entire contacting surface of the device with a dense arrangement of actuators can affect its normal use. Determining how to produce desired vibration patterns at any contact point with only a few sparse actuators deployed on the surface of the handheld device remains a significant challenge. In this work, we develop a tactile feedback board in the size of a smartphone with only five actuators, and achieve the precise production of vibration patterns that can focus at any desired position on the board. Specifically, we investigate the vibration characteristics of a single passive coil actuator and construct its vibration pattern model for any position on the feedback board surface. Optimal phase and amplitude modulation, determined using the simulated annealing algorithm, is employed with five actuators in a sparse array. The vibration patterns from all actuators are superimposed linearly to synthetically generate different onboard vibration energy distributions for tactile sensing. Experiments demonstrated that point-wise vibration pattern production on our tactile board achieved an average level of about 0.9 in the Structural Similarity Index Measure (SSIM) evaluation, when compared to the ideal single-point-focused target vibration pattern. Four point-wise patterns focused on the top, bottom, left, and right parts of the tactile board were applied, to guide continuous directional movements without visual assistance, which shows significant implications for machine-assisted cognition based on vibration tactile feedback.**

I. Introduction

Human integrates touch and vision in a statistically optimal way for estimating the properties of objects, and programmable tactile feedback can convey the rich touch sensory information thus covering the gap of visual sense in some scenes [1]. Vibration is the most common form of tactile feedback, due to its advantages including noticeable effects, simple generation, easy deployment, and resilience to environmental interference [2], [3]. Incorporating vibration pattern feedback into handheld devices, like smartphone, touch panel and game controller, can help to achieve precise manipulation [4], as well as to enhance the interaction immersion [5]. And it has held promising applications in social and personal engagement [6], touch control and feedback [7], and gaming and entertainment [8]. However, for these handheld devices, it is challenging to deploy a dense actuator array like in [9]–[12] to cover the whole surface, which would perform a great negative effect on the device manipulation.

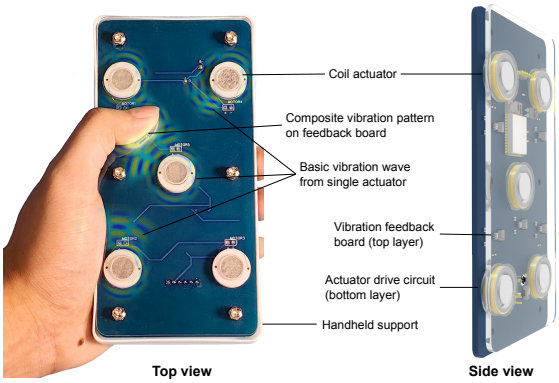

Fig. 1. Point-wise vibration pattern feedback superimposed by the sparse actuator array on the top feedback board, with the bottom circuit board for actuator voltage driving.

In recent years, researchers have attempted to leverage the tactile funneling illusion [13], [14] and vibration-induced location illusion [15], [16], to generate the specific vibration pattern by wave superposition using actuators with a limited amount. Seo *et al.* [17] firstly investigated the tactile phantom sensation between two tactile actuators by manipulating vibration rendering, duration and direction, to create various sensations of vibration position and intensity. Then they designed 32 different types of the edge-flow vibration patterns, and achieved an information transmission capacity of 3.70 bits [18]. Pantera *et al.* [19], [20] employed the inverse filtering method to decouple multi-point vibration modes in a sparse actuator array, enabling individual fingers to feel different vibration modes. To address the distortion in target vibration points within vibration patterns, Vlam *et al.* [21] tried to focus the energy by utilizing the vibration wave propagation and attenuation, and achieved the generation of 9 vibration target locations within the scope of four sparse actuators. These efforts on the sparse actuator array, also including [22]–[24], have achieved the area-specfic vibration pattern production with a number of distinguishable species that far exceeds that of actuators. However, for any contacting point on the two-dimensional tactile feedback surface, the point-wise vibration pattern production via only a few sparse actuators still needs further research.

In this study, we develop a surface tactile board based

†These authors contributes equally to this article.

X. Li, R. Zhao, C. Lu, X. Xiao, and W. Ding are with Tsinghua-Berkeley Shenzhen Institute, Tsinghua Shenzhen International Graduate School, Tsinghua University, China. W. Ding is the corresponding author. E-mail: ({lixs21, zhaorz22, xiaox22}@mails.tsinghua.edu.cn, {luchengyue, ding.wenbo}@sz.tsinghua.edu.cn). W. Ding is also with RISC-V International Open Source Laboratory, Shenzhen, China, 518055.

This article has supplementary materials of hardware and software available at https://github.com/Lixiaosa1996/VibrationPattern.git.

on the sparse actuator array as shown in Fig. 1, to provide point-wise vibration feedback on the contacting fingertip of handheld users. Five passive coil actuators with the same specification are uniformly distributed on the tactile board in the smartphone size. For single actuator with the flap-latch structure, sine wave in the frequency of 160 Hz is chosen as basic vibration wave for modulation, which owns the maximum resonant energy. According to the homogeneity and superposition of five actuator vibration patterns, we model the tactile feedback board as a Linear Time-Invariant (LTI) system with the input of single actuator vibration mode. By driving each actuator with the basic sine wave of modulated phase spectrum, vibration patterns on the board are superimposed as different energy distribution images. For the target point-wise vibration pattern production, we employ the simulated annealing algorithm to search the optimal phase spectrum for every actuator, to ensure the composite vibration energy image to have the max Structural Similarity Index Measure (SSIM) value with the target image. For random target feedback point on the board, our strategy can reach an average value of about 0.9 in the SSIM evaluation. And four different point-wise vibration feedback pattern were used to deliver touching messages of directions to the handheld users, for the vibration guided movements without vision and an immersive tactile feedback experience.

The main contributions of this article are as follows:

- For single actuator, vibration characteristic analysis with the passive flip-latch structure is elaborated by acceleration measurement, mainly about the tactile feedback board responses to varying vibration frequencies and waves for driving the actuator.
- For the vibration feedback board, we have built a LTI system model with the input value of single actuator vibration pattern series in the timeline. This is based on the proof of the homogeneity and the superposition inherent to the vibration patterns for different actuators.
- For onboard vibration pattern production, point-wise vibration pattern decoupling is achieved with the random search of simulated annealing in the phase space of five actuators. By constantly getting out of local optimal solutions for actuator phase spectrum, the vibration energy distribution should finally focus on the target feedback point.

II. Coil Actuator Specification

Coil actuators serve as a crucial component for generating vibration feedback on the surface of tactile board. To facilitate full control over the vibration wave, eccentric-structure-based vibration motor with the fixed motor and frequency is eschewed, and magnet-coil assemblies utilizing a flip-latch structure is designed as depicted in Fig. 2(A). In each coil actuators, the copper wire with a diameter of 0.1 mm is wound 150 turns around an I-shaped frame, forming a hollow cylindrical coil with inner diameter of 13 mm, outer diameter of 17 mm, and height of 2 mm, which is securely affixed to the bottom current-driving circuit board. the cylindrical permanent magnet core, with a diameter of 10 mm and height of 4 mm, is situated in the center of the cooper coil, but remains non-contacting. When the coil is energized by an alternating voltage, the magnet core experiences alternating attraction and repulsion under the coil magnetic field, driving the attached acrylic tactile board in upward and downward motions to generate vibration feedback. In the latch structure, the magnet core and the coil maintain their relative positions between the top vibration board and the bottom circuit board in the static status. And the magnet core can reach a large range of vertical travel, and do incur little energy loss compared to the flexible silicone support in the typical cantilever-beam structure.

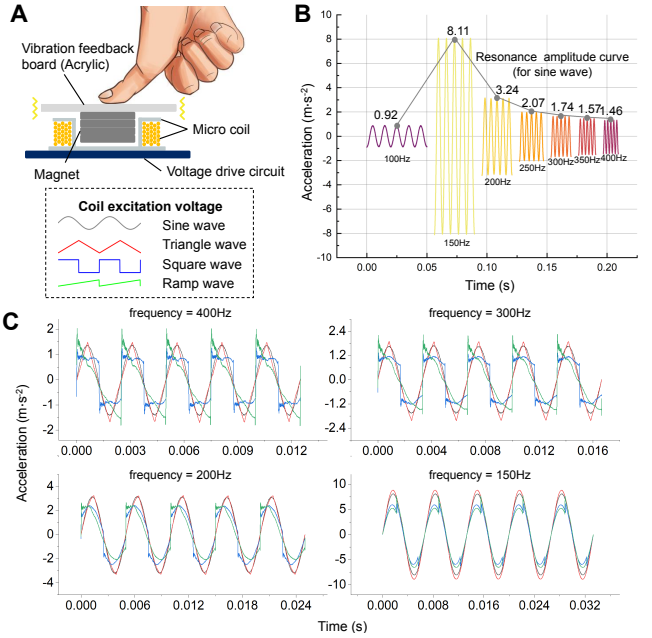

Fig. 2. Specification of single coil actuator. (A) Flip-latch structure for actuator. (B) Resonance energy variation for vibration drive sine wave in the sweep frequency. (C) Time-domain vibration response in the acceleration form on the feedback board, for sine, triangle, square, and ramp wave driving in the sweep frequency, respectively.

In our control setup, we deployed an ESP32-Wroom-32D micro-controller within the voltage drive circuit for Pulse Width Modulation (PWM) signal emission, emulating a variety of waveforms including sine, triangle, square, and ramp waves, with the amplified control of coil actuators through the field-effect tube FS8205a. Configuration of the original drive wave frequency and duty cycle is managed on the host computer and communicated to the drive board for PWM output in real-time via the User Datagram Protocol (UDP) within the local network, enabling the operation of five actuators at 10 kHz, with minimal network latency of 10 ms.

Selected drive waves ranging from 100 to 400 Hz were applied to the passive coil actuators. We gathered acceleration data at the tactile board's fingertip contact area using a high-resolution piezoelectric accelerometer (SAED0005B, Wuxi Shiao). This data validated the vibratory response of the actuators to varying voltage inputs and demonstrated that the

maximum vibratory response across all selected waveforms occurred at 160 Hz, the natural resonance frequency of the tactile board. These findings are graphically represented in Fig. 2(B) and (C). Around 160 Hz, we observed a convergence in waveform responses towards a sinusoidal shape, regardless of the initial waveform, with the sine wave maintaining maximum amplitude. Beyond the resonant frequency, the vibration response increasingly resembles the input waveform, particularly at higher frequencies. The data thus suggests that the 160 Hz sine wave is the most effective for driving the tactile board's actuators, yielding the most efficient vibration feedback.

III. Vibration Board Modeling

The tactile feedback board employed in this article is fabricated from a 1 m-thin acrylic sheet with dimensions 71.5×146.7 mm^2. When vibration generating, the permanent magnet within the coil actuator is subjected to the coil alternating magnetic field, causing vertical motion that induces bending deformations at the corresponding locations on the thin elastic acrylic board. At a actuator vibration frequency of f(=160 Hz), the bending wavelength of the board vibration is approximately 187 mm, substantially greater than its thickness. Therefore, we can qualify the plate as an isotropic and homogeneously thin elastic plate.

A. Vibration Pattern of Single Actuator

Note the position of single actuator on the vibration board as (x_0, y_0), and the drive wave amplitude for vibration induced on the thin plate is $F(t) = A\cdot \sin(2\pi ft+\phi)$. Considering that the displacement is $w(x, y, t)$ at any observation position (x, y) on the vibration feedback board at any time t within the board boundaries $(0 \le x \le a, 0 \le y \le b)$. The board's motion can be described by the dynamic Kirchhoff plate model, taking into account the plate's bending stiffness, which is influenced by both its own mass and external loading. The governing equation for the motion of the whole vibration board is represented as:

$$D\nabla^4 w + \rho h\frac{\partial^2 w}{\partial t^2} = F(t)\delta(x-x_0)\delta(y-y_0), \qquad (1)$$

where $D = Eh^3/(12(1-\nu^2))$ denotes the flexural rigidity of the plate, a function about the thickness h, Young's modulus E, and Poisson's ratio ν. Here, ∇^4 is a bi-harmonic operator, and $D\nabla^4 w$ represents the plate's restoring force under the influence of external loads. ρ and h are the density and thickness of the plate respectively, and $\frac{\partial^2 w}{\partial t^2}$ reflects the plate's inertia. δ is the Dirac delta function, implying the external load only exists at the actuator position (x_0, y_0).

Throughout the vibration process, each mode of the vibration feedback board has its specific spatial distribution and time dependency. Their product indicates the contribution of this spatio-temporal mode to the overall displacement of the board. The displacement $w(x, y, t)$ at any point and time can be viewed as the superposition of all spatio-temporal modes. Based on the properties of the partial differential equation, the displacement can be written as an eigenfunction expansion in the modal space:

$$w(x, y, t) = \sum_{m=1}^{\infty}\sum_{n=1}^{\infty}\phi_{mn}(x, y)q_{mn}(t). \qquad (2)$$

Here, m and n serve as the modal coordinates. $\phi_{mn}(x, y)$ is the eigenfunction representing the spatial distribution (modal shape function) of mode (m, n) for the feedback board. And $q_{mn}(t)$ denotes the time-dependent coefficient representing the amplitude variation of the corresponding mode at the corresponding time.

To obtain the spatial vertical displacement response $w(x, y, t)$ of the vibration feedback board at any given time t, we need to sum over the terms $\phi_{mn}(x, y)$ and $q_{mn}(t)$ in the space and time domain. By solving Eqn. (2), we can generate a graphical representation of the vibration state of the entire feedback plate at arbitrary time instants. As an example, the vibration pattern at a specific time instance within a stable periodic cycle for the middle Actuator 3 with a phase of 0 is depicted in Fig. 3(A) at a resolution of 179×367 points.

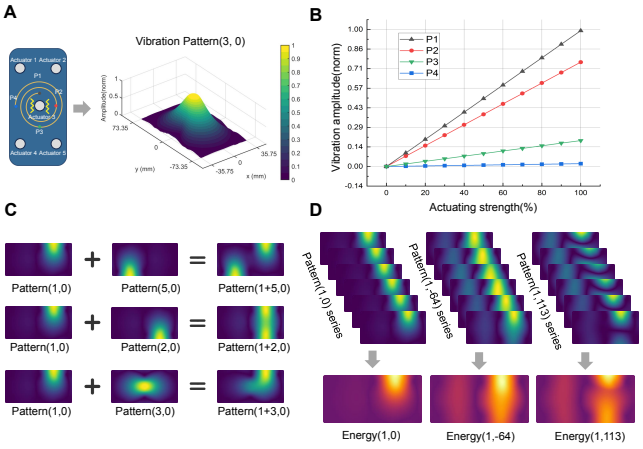

Fig. 3. Modeling of the vibration feedback board system. (A) Vibration pattern generation for single actuator. (B) The linearity between the onboard vibration amplitude and the actuator driving strength. (C) Superposition of vibration pattern form different actuators. (D) Transfer the vibration patterns in single period to the energy distribution image, for satisfying the human tactile perception ability.

B. Homogeneity and Superposition of Multiple Patterns

In the aforementioned comprehensive solution process, the time-dependent coefficient $q_{mn}(t)$ exhibiting a linear relationship to the drive wave amplitude $F(t)$ under the sinusoidal shape. And this homogeneity remains between the amplitude of the vibration response $w(x, y, t)$ and the drive wave. This linear relationship was empirically verified by measuring the amplitudes at various observation points located at different distances and directions around Actuator 3, as shown in Fig. 3(B). Within the range of vibration intensities that can be applied by the vibration board, a consistent linear correlation has been maintained between the amplitude of the actuator driving wave and the vibration feedback. For any single actuator $i \in \{1, 2, 3, 4, 5\}$, the

vibration pattern $\mathbf{P}$ under the driving wave of amplitude A and phase ϕ is represented, in light of this linearity, as $A \cdot \mathbf{P}(i, \phi)$.

The vibrating plate used in this study is made of uniform acrylic material, and the vibration patterns induced by different coil actuators can be directly summed at any given time instant to produce a composite vibration pattern. We have validated this superposition relationship of vibration patterns originating from different actuators, as demonstrated in Fig. 3(C). By independently driving Actuator 1 and its opposite, diagonal, and central actuators, their time-sequential vibration patterns is numerically summed within a stable cycle. The result is found to be entirely consistent with the time-sequential vibration patterns obtained by two simultaneously-driving actuators. In rigorous mathematical terms, the composite vibration profile, generated by the simultaneous operation of multiple actuators $i_1, i_2, \ldots, i_n$ with amplitudes $A_1, A_2, \ldots, A_n$ and phases $\phi_1, \phi_2, \ldots, \phi_n$, can be expressed as the linear combination of their individual contributions. Specifically, we denote this property of additive superposition of vibration patterns from disparate sources, along with the linearity, as the formula:

$$\begin{aligned} \boldsymbol{A} \cdot \mathbf{P}([i_1, i_2, \ldots, i_n], [\phi_1, \phi_2, \ldots, \phi_n]) = \\ A_1 \cdot \mathbf{P}(i_1, \phi_1) + A_2 \cdot \mathbf{P}(i_2, \phi_2) + \cdots + A_n \cdot \mathbf{P}(i_n, \phi_n). \end{aligned} \tag{3}$$

Human vibration perception exhibits a specific sensitivity across different dimensions such as frequency, amplitude, and waveform. The perception is particularly acute within the frequency range of 20∼500 Hz. However, for the 160 Hz high-frequency sinusoidal wave employed on this vibration board, it is challenging to discern waveform variations in the time domain resulting from phase modulation. Under this circumstance, the sensation induced by the 160 Hz vibration resembles fluctuations in a form of energy rather than the wave shape. For the single-period vibration pattern series, the Root Mean Square (RMS) of the vibration amplitude at each point in the spatial frame is calculated over time, serving as a measure as the vibration energy distribution image with the same size of vibration pattern. The vibration energy distribution $\mathbf{E}$ across the entire tactile feedback board can be represented as follows:

$$\mathbf{E} = \mathrm{RMS}(\mathbf{P}). \tag{4}$$

Accordingly, vibration pattern sequences can be transformed into energy images that better quantify the human tactile perception characteristic, as shown in Fig. 3(D). Even unlike the original vibration patterns with both positive and negative value, vibration energy images lack polarity but retain high similarity with the original patterns. Besides, vibration energy image elucidates the clear impact of drive wave phase on the final vibration pattern. Even for the same actuator, different phases of the sinusoidal driving waveform result in distinct vibration energy images due to differing initial conditions. This diversity enriches the basic vibration modes emanating from a sparse array of actuators, enabling the superposition of targeted single-point vibration pattern feedback by modulating the phase spectrum of each actuator.

IV. Vibration Pattern Decoupling

When vibration waves originating from five actuators propagate from disparate locations, and converge at a specific point on the vibration feedback board, their induced longitudinal displacements sum up in accordance with the principle of linear superposition. And this superposition process is reversible for the LTI vibration system. It implies that for a vibration distribution image with an arbitrary target point as the source, it is possible to decouple the contributions from vibration waves emanating from a sparse array of actuators.

The generation of the target vibration energy distribution, $\mathbf{E}_T$, serves as the initial step in the entire process of vibration pattern decoupling. To ensure the reversibility of the vibration synthesis and decoupling process, the target energy distribution must be derived from the vibration patterns of single-point vibration source. For any target vibration feedback point $\boldsymbol{T}(x_T, y_T)$, Eqn. (2) is employed to solve for the vibration patterns of single actuator at position $\boldsymbol{T}$. Then, the target vibration energy distribution, $\mathbf{E}_T$, is obtained by taking the RMS value of the vibration energy at each point across the vibration feedback board by Eqn. (4).

During the process of vibration decoupling, we select unit-amplitude vibration pattern sequences from five actuators, each at all 360 phases by one degree, as the basic vibration modes. By adjusting each basic vibration mode with the respective amplitude (constrained to be within ten times the unit amplitude), we synthesize the vibration pattern sequences across the entire feedback board according to Eqn. (3). The final objective of the decoupling process is to make the energy distribution $\mathbf{E}$, of the synthesized vibration pattern , as similar as possible to the target energy distribution $\mathbf{E}_T$. Here, we choose the SSIM as the evaluation metric, with a particular focus on the contrast of vibration energy on different areas. Within the range from 0 to 1, the closer the SSIM value between the synthesized and target vibration energy distributions approaches 1, the more effective is the generated vibration pattern effect.

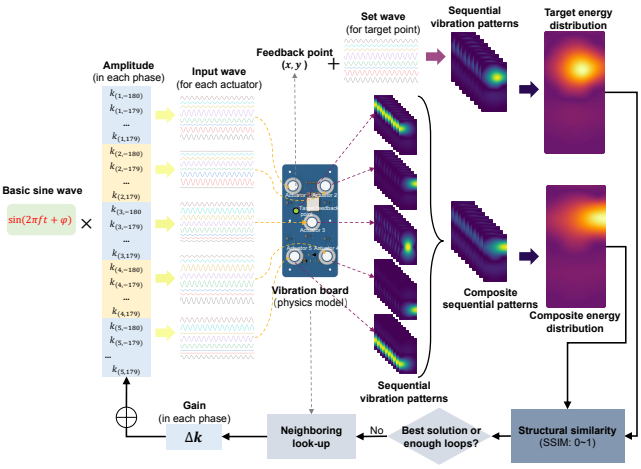

Fig. 4. The global optimal amplitude spectrum searching in all phases for each actuator, based on the vibration superposition model and the simulated annealing algorithm.

For the vibration pattern decoupling, the efficacy evaluation is based on the energy distribution image, whereas the vibration synthesis process is reliant on the sequence of vibration patterns. Consequently, this decoupling problem is not amenable to gradient descent or machine learning-based optimization methods. During the application of stochastic search algorithms, it is crucial to consider that the vibration decoupling problem might possess multiple optimal solutions, necessitating a strategy to avoid the entrapment in local optima. For the synthesized and target energy images, their SSIM value can be construed as a form of energy. Throughout the optimization process, the similarity value incrementally ascends from a lower level to achieve the stabilization at a high level, allowing for the possibility of escaping local optima through an approach analogous to simulated annealing. Specifically, when the SSIM value is low, the optimization process is configured to accept bad solutions at the current step with a relatively high probability. The entire vibration energy distribution decoupling process based on the simulated annealing approach is detailed in **Algorithm** 1 and Fig. 4.

Algorithm 1: Vibration Energy Distribution Decoupling.

Input: Basic vibration pattern series for 5 coil actuators in the 360 phases: $\mathbf{P}(i,j)$; Target vibration feedback point:(x_T, y_T).

Output: Amplitude gain coefficients for each coil actuator in its all phases: $\boldsymbol{k}(i,j)$, which makes the composite vibration pattern closest to the target pattern.

Simulate the target vibration energy distribution $\mathbf{E}_T$;
Initialize all the gain coefficients $\boldsymbol{k}_0(i,j)$ randomly;
Get the energy distribution of initial composite patterns $\mathbf{E}_0\,(\boldsymbol{k}_0 * \mathbf{P})$;
while n **in** range(10000) **do**
  Generate the all the gain offset $\boldsymbol{k}_n = \boldsymbol{k}_{n-1} + \Delta\boldsymbol{k}$;
  Add the basic vibration patterns with gain $\boldsymbol{k}_n * \mathbf{P}$;
  Get the energy of composite patterns $\mathbf{E}_n\,(\boldsymbol{k}_n * \mathbf{P})$;
  Compute the energy distribution similarity $\mathrm{SSIM}\,(\mathbf{E}_n, \mathbf{E}_0)$;
  if $\mathrm{SSIM}\,(\mathbf{E}_n, \mathbf{E}_0) < \mathrm{SSIM}\,(\mathbf{E}_{n-1}, \mathbf{E}_0)$ **or** $1 - \mathrm{SSIM}\,(\mathbf{E}_{n-1}, \mathbf{E}_0) < \mathrm{rand}(0,1)$ **then**
    Accept this new gain offset of $\Delta\boldsymbol{k}$;
  else
    Do not update the gain $\boldsymbol{k}_n = \boldsymbol{k}_{n-1}$;
Output the locally optimal solution for amplitude gain coefficients $\boldsymbol{k}(i,j) = \boldsymbol{k}_{10000}$

V. Experiments and Results

During the experiment process, vibration patterns at several different position were generated and calculated as the target energy distributions. Vibration pattern sequences originating each of 5 actuators for all 360 phases within single period, were stored as fundamental vibration modes. Leveraging the homogeneity and superposition properties of our feedback board, these fundamental vibration modes were linearly combined using the optimal phase spectrum for actuators obtained through the vibration decoupling process, and then a synthesized vibration energy image that approximates the target single-point vibration feedback was obtained.

A. Vibration Pattern Generation

The effectiveness of generating point-wise vibration image on the tactile feedback board is illustrated in Fig. 5(A). Taking four random target feedback points as examples, the SSIM value between the synthesized vibration image obtained through vibration decoupling and the target single-point vibration image ranged between 0.85 and 0.95. In each synthesized vibration image, the focal point of energy concentration in the synthesized vibration feedback closely approximated the target vibration feedback point, without any energy concentration in other areas. The localized composite vibration energy distribution demonstrates the superiority of the vibration decoupling method proposed in this study. And the target vibration energy distribution for the first target point (10, 25), achieved through the superposition of different vibration patterns emanating from five actuators, is shown in Fig. 5(B).

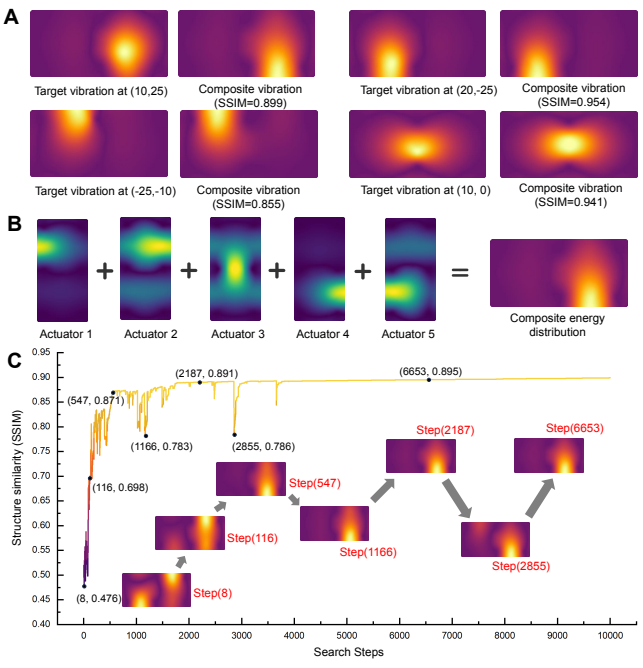

Fig. 5. Effect of point-wise vibration pattern generation on the tactile feedback board. (A) Comparison between composite vibration energy pattern and target pattern for different target feedback points. (B) Raw vibration patterns from five actuators are superimposed as the optimal energy distribution image closet to the target pattern. (C) SSIM value promotion of vibration energy distribution during the simulated annealing search process.

Taking the vibration image decoupling at the target point (10, 25) as an example, we plotted the process of simulated annealing to search for the closest vibration energy image

in Fig. 5(C), which was able to be completed in 8∼9 hours. A randomly initialized phase spectrum was selected as the initial solution, where the SSIM value was 0.476 at Step(8). As the search process progressed, energy concentration areas far from the target feedback point gradually disappeared, and the SSIM index increased to 0.698 at Step(116). Then, by overcoming several local optimal values, the only energy concentration point progressively approached the target position, and the SSIM similarity index had risen to 0.871 by Step(547). In the subsequent search process, the optimal synthesized energy image had essentially stabilized, with the SSIM value remaining around 0.9 due to minor parameter adjustments in the search process. At this point, the algorithm had approximated the global optimum solution, achieving the maximum similarity between the synthesized vibration image and the target point vibration image. And point-wise vibration pattern production at any location of the tactile board surface was able to be achieved through this vibration decoupling process.

B. Vibration Pattern based Navigation

In the application experiment, we attempted to guide the user's motion using different point-wise vibration patterns without any other senses. Four produced vibration patterns, focusing on the top (0,25), bottom (0,-25), left (-20,0), and right (20,0) part of the tactile feedback board, were used to indicate the walking directions of forward, backward, left, and right, respectively. We first tested the recognition accuracy and corresponding recognition time of the four vibration patterns played randomly, as shown in Fig. 6(B) and (C) while the tactile board was handheld with full contact between the user's thumb and the board surface. Each vibration pattern was tested by 100 times, and every recognition accuracy was over 90%, with the respective average recognition times of 1.80s, 2.22s, 2.66s, and 2.33s. And it showed that the left and right vibration patterns were more likely to be misidentified due to the proximity of their focus points. Then, a blindfolded volunteer was required to perform continuous single-step walking movements under the guidance of four vibration patterns, including several alternating advances, lateral movements, and retreats in Fig. 6(E). Throughout the whole movement process, we found that the user was still able to maintain a high accuracy in recognizing the handheld vibration patterns, as well as the rapid recognition within seconds, which has demonstrated the effectiveness of our vibration pattern production for conveying complex tactile messages in handheld devices.

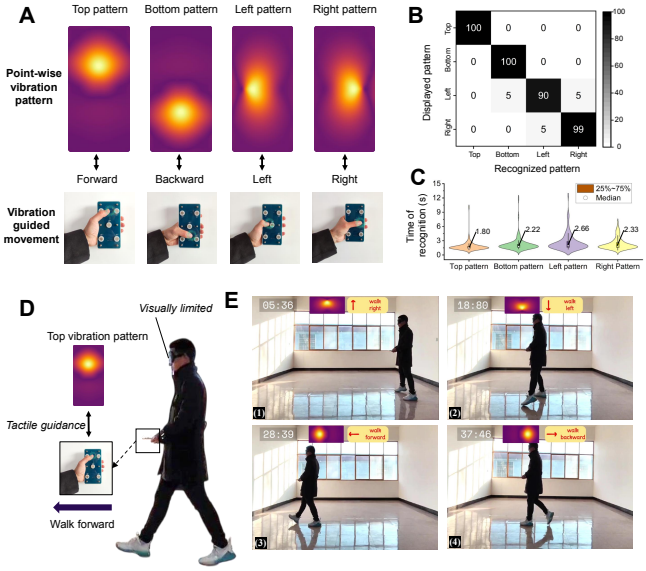

Fig. 6. Four different point-wise vibration patterns guided directional movements. (A) Vibration patterns focused on the top, bottom, left, and right part on the tactile board, convey the messages of forward, backward, left, and right movements respectively. (B) Confusion matrix for four vibration patterns recognition. (C) Violin plots for the time required of each pattern's recognition. (D) The conceptual diagram of vibration-guided movements with limited vision. (E) The blindfolded user walked toward different direction in a continuous motion under the guidance of four varying vibration patterns on our handheld tactile board.

VI. Conclusion

In this study, we introduce a method for generating focused single-point vibration feedback on a tactile board using phase-modulated driving waves in a sparse array of actuators. We determined that a 160 Hz sine wave, chosen for its maximal resonance energy, is optimal for driving a single coil actuator with a flip-latch structure. This discovery facilitated the development of a linear time-invariant (LTI) system model for synthesizing vibration patterns through superposition and verified homogeneity. Utilizing simulated annealing for optimal phase determination, we modulated this sine wave to concentrate vibration energy effectively at the desired feedback points, achieving high Structural Similarity Index Measure (SSIM) values. Concisely, by measuring single-actuator vibrations, we eliminated ineffective modulation parameters such as basic waveforms and frequencies. This linear synthesis model expedited the search for the optimal phase spectrum, enabling it to conclude within hours. We can pre-store this optimal phase spectrum in a lookup table for any given point, allowing handheld devices to rapidly focus vibration energy at a targeted location. Thus, we demonstrate that sparse actuator arrays can provide precise, position-specific vibration feedback for tactile guidance in handheld devices.

VII. Acknowledgment

This work was supported by Shenzhen Ubiquitous Data Enabling Key Lab under Grant No. ZDSYS20220527-171406015, by Guangdong Innovative and Entrepreneurial Research Team Program (2021ZT09L197), by Shenzhen Science and Technology Program (JCYJ20220530143013030), by Tsinghua Shenzhen International Graduate School and Shenzhen Pengrui Young Faculty Program of Shenzhen Pengrui Foundation (No. SZPR2023005). We also extend our thanks to Qianqian Tong from Pengcheng Laboratory for her editorial assistance with the manuscript and to Tengbin Jiang from Southwest University of Political Science and Law for his help with the application experiments.

REFERENCES

[1] M. O. Ernst and M. S. Banks, "Humans integrate visual and haptic information in a statistically optimal fashion," *Nature*, vol. 415, no. 6870, pp. 429–433, 2002.

[2] A. E. Sklar and N. B. Sarter, "Good vibrations: Tactile feedback in support of attention allocation and human-automation coordination in event-driven domains," *Hum. Factors*, vol. 41, no. 4, pp. 543–552, 1999.

[3] M. C. Jimenez and J. A. Fishel, "Evaluation of force, vibration and thermal tactile feedback in prosthetic limbs," in *IEEE Haptics Symp. (HAPTICS)*, Doha, Qatar, Jun 2014, pp. 437–441.

[4] D. Croce, L. Giarré, F. G. La Rosa, E. Montana, and I. Tinnirello, "Enhancing tracking performance in a smartphone-based navigation system for visually impaired people," in *Mediterr. Conf. Control Autom. (MED)*, Athens, Greece, Jun 2016, pp. 1355–1360.

[5] D. S. Pamungkas and K. Ward, "Electro-tactile feedback system to enhance virtual reality experience," *Int. J. Comput. Theory Eng.*, vol. 8, no. 6, pp. 465–470, 2016.

[6] Y. Ding, C. Shultz, and C. Harrison, "Surface I/O: Creating devices with functional surface geometry for haptics and user input," in *Conf. Hum. Fact. Comput. Syst. Proc. (CHI)*, Hamburg, Germany, Apr 2023, pp. 1–22.

[7] Y. Chen, X. Liang, S. Chen, Y. Chen, H. Lin, H. Zhang, C. Jiang, F. Tian, Y. Zhang, S. Yao *et al.*, "HapTag: a compact actuator for rendering push-button tactility on soft surfaces," in *ACM Symp. User Interface Softw. Technol. (UIST)*, Bend, United States, Oct 2022, pp. 1–11.

[8] P.-H. Han, Y.-S. Chen, K.-T. Yang, W.-S. Chuan, Y.-T. Chang, T.-M. Yang, J.-Y. Lin, K.-C. Lee, C.-E. Hsieh, L.-C. Lee *et al.*, "Boes: attachable haptics bits on gaming controller for designing interactive gameplay," in *ACM Spec. Int. Grp. Comp. Graph. Interact. Tech. (SIGGRAPH)*, Los Angeles, United States, Jul 2017, pp. 1–2.

[9] X. Yu, Z. Xie, Y. Yu, J. Lee, A. Vazquez-Guardado, H. Luan, J. Ruban, X. Ning, A. Akhtar, D. Li *et al.*, "Skin-integrated wireless haptic interfaces for virtual and augmented reality," *Nature*, vol. 575, no. 7783, pp. 473–479, 2019.

[10] K. Yao, J. Zhou, Q. Huang, M. Wu, C. K. Yiu, J. Li, X. Huang, D. Li, J. Su, S. Hou *et al.*, "Encoding of tactile information in hand via skin-integrated wireless haptic interface," *Nat. Mach. Intell.*, vol. 4, no. 10, pp. 893–903, 2022.

[11] Y. Guo, Q. Tong, X. Liu, X. Bian, Z. Zhang, Y. Zhang, W. Xu, and D. Wang, "MRS-Tex: A magnetically responsive soft tactile device for texture display," *IEEE Trans. Ind. Electron.*, vol. 69, no. 11, pp. 11 531–11 540, 2021.

[12] Y. Guo, Q. Tong, P. Zhao, Y. Zhang, and D. Wang, "Electromagnetic-actuated soft tactile device using a pull-push latch structure," *IEEE Trans. Ind. Electron.*, vol. 70, no. 10, pp. 10 344–10 352, 2023.

[13] D. S. Alles, "Information transmission by phantom sensations," *IEEE Trans. Hum.-Mach. Syst.*, vol. 11, no. 1, pp. 85–91, 1970.

[14] L. A. Jones and S. J. Lederman, *Human hand function*. Oxford University Press, 2006.

[15] J. Dargahi and S. Najarian, "Human tactile perception as a standard for artificial tactile sensinga review," *Int. J. Med. Robot. Comp.*, vol. 1, no. 1, pp. 23–35, 2004.

[16] S. J. Lederman and R. L. Klatzky, "Haptic perception: A tutorial," *Atten. Percept. Psychophys.*, vol. 71, no. 7, pp. 1439–1459, 2009.

[17] J. Seo and S. Choi, "Initial study for creating linearly moving vibrotactile sensation on mobile device," in *IEEE Haptics Symp. (HAPTICS)*, Washington, United States, 2010, pp. 67–70.

[18] ——, "Edge flows: Improving information transmission in mobile devices using two-dimensional vibrotactile flows," in *IEEE World Haptics Conf. (WHC)*, Chicago, United States, Jun 2015, pp. 25–30.

[19] L. Pantera and C. Hudin, "Sparse actuator array combined with inverse filter for multitouch vibrotactile stimulation," in *IEEE World Haptics Conf. (WHC)*, Tokyo, Japan, Jul 2019, pp. 19–24.

[20] ——, "Multitouch vibrotactile feedback on a tactile screen by the inverse filter technique: Vibration amplitude and spatial resolution," *IEEE Trans. Haptics*, vol. 13, no. 3, pp. 493–503, 2020.

[21] V. de Vlam, M. Wiertlewski, and Y. Vardar, "Focused vibrotactile stimuli from a wearable sparse array of actuators," *IEEE Trans. Haptics*, 2023, to be published.

[22] D. Ryu, G.-H. Yang, and S. Kang, "T-hive: Vibrotactile interface presenting spatial information on handle surface," in *IEEE Int. Conf. Rob. Autom. (ICRA)*, Kobe, Japan, May 2009, pp. 683–688.

[23] J. Kang, J. Lee, H. Kim, K. Cho, S. Wang, and J. Ryu, "Smooth vibrotactile flow generation using two piezoelectric actuators," *IEEE Trans. Haptics*, vol. 5, no. 1, pp. 21–32, 2012.

[24] C. Basdogan, F. Giraud, V. Levesque, and S. Choi, "A review of surface haptics: Enabling tactile effects on touch surfaces," *IEEE Trans. Haptics*, vol. 13, no. 3, pp. 450–470, 2020.